Reciprocity calibration method for ultrasonic piezoelectric transducers in air. Comparison of finite element modelling and experimental measurements

Andersen, K. K.*[a], Søvik, A. A.[a], Lunde, P.[a,b,c], Vestrheim, M.[a,c], and Kocbach, J.[b,c]

[a]*University of Bergen, Department of Physics and Technology, Postboks 7803, NO-5020 BERGEN, Norway*
[b]*Christian Michelsen Research AS (CMR), P.O. Box 6031 Postterminalen, NO-5892 BERGEN, Norway*
[c]*The Michelsen Centre for Industrial Measurement Science and Technology, PO. Box 6031, NO-5892 Bergen, Norway*

Abstract

A modified free- and far-field three-transducer reciprocity calibration method has been utilized to determine the receiving voltage sensitivity, M_V, of a piezoelectric disc. The measurement results are compared to finite element modelling (FEM). A system model has been employed to give a theoretical description of the measurement system at hand, allowing corrections to be made accounting for laboratory instrumentation, diffraction and attenuation in air.

A technique to isolate different noise contributors has been utilised to obtain two different signal-to-noise ratio (SNR) analyses. It is shown that the SNR given coherent noise drops significantly, compared to that of random noise, for a certain frequency range when the piezoelectric discs are moved closer together.

All work is performed on piezoelectric discs radiating in air at room temperature at approximately 1 atm, with the first radial mode, R1, at about 100 kHz. The frequency range of interest is 100-300 kHz, though only a subset of this, 50-140 kHz, is investigated in the current work.

I. Introduction

The use of ultrasound in the industry motivates the study of calibration of precision measurement equipment operating in air in the frequency range 100-300 kHz. Industrial usages of ultrasound in this frequency range can be e.g. fiscal measurement of natural gas, therein multipath ultrasonic transit-time flow meters (USM) [1], measurements of the velocity of sound in the gas (VOS) [1], as well as quality measurements on natural gas [2] and air-coupled non-destructive testing (NDT) [3].

Although some techniques for the calibration of air microphones in the audio frequency range were developed before the 1940s [4], the calibration of electroacoustic transducers by the reciprocity method began shortly after 1940 with the independent work of MacLean [5] and Cook [6].

The free-field three-transducer reciprocity calibration method has since been adopted e.g. by the American National Standards (ANSI) [7], [8] and the International Electrotechnical Commission (IEC) [9].

In [10] the three-transducer reciprocity calibration technique was used over the frequency range 100-500 kHz for transducers operating in air. Broadband electrostatic transducers were employed [10], [11] to obtain the receiving voltage sensitivity, M_V, and the transmitting voltage response, S_V. Challenges related to the use of the three-transducer calibration technique at such high frequencies was with the use of corrections for diffraction and attention in air. Although, corrections for the signal filter were made, and it is stated [10] that parasitic current losses were less than 0.2 percent from the ideal open circuit conditions, no system model was employed.

*E-mail: kan091@student.uib.no / kenneth.kirkeng.andersen@gmail.com

In [12] and [13] (both partly presented in [14], [15] and [16]) a finite-element (FE) based system model was employed, for calculations of correction terms to the measurements, and as an aid for improved control in evaluating the quality of the individual measurements constituting the three-transducer calibration method.

In [12] the three-transducer calibration method was employed to obtain M_V and S_V of piezoelectric discs and in-house built transducers, and the results were compared to FE simulations.

Although an adjusted material data set [17] was used in [12] and [13] to model the piezoelectric discs, the adjusted data set was not obtained for the specific piezoelectric discs used in the measurements. Contrary to this, the corrected measurements and the corresponding simulated quantities agreed fairly well.

Furthermore, for the piezoelectric discs, it was found that the corrections for absorption in air, on both M_V and S_V approached 6 dB at 300 kHz. And, around 112 kHz, the corrections for the receiving electronics approached 8 dB. The latter also introduced a frequency shift on the peak value of the receiving voltage sensitivity of up to several kHz.

In [12] this implementation of the three-transducer calibration method was also tested on a pre-calibrated B&K microphone system 4138-A-015 [18] and found to lie within 1 dB of the supplied calibration data for the frequency range 103-130 kHz [12], indicating that the corrections applied to the measurements are reasonable.

The phase response of M_V, S_V or the involved voltage to voltage transfer function was not addresses in neither [10], [12] nor [13].

When modelling in a finite element environment, detailed knowledge about the material parameters for the materials involved in the modelled construction is necessary for accurate results. When using commercial transducers, little information regarding the different materials involved in the transducer construction is available [17]. When modelling in-house built transducers, lack of reliable and accurate material data for the materials involved, e.g. glue, metal housing, front- and back layer, can also pose challenges [19]. Prior work at the University of Bergen (UiB) on piezoelectric discs have shown fair agreement between measurements and simulations [17], while the same comparison on in-house built transducers has provided more challenges [12], [13].

Only piezoelectric discs are considered in the current work. The piezoelectric discs under investigation has a D/T-ratio of about 10, with the first radial mode, $R1$, around 100 kHz. The lower radial modes in the piezoelectric discs are investigated since these modes are frequently used in transducers for gas operating in the frequency range 100-300 kHz. Other candidate modes, e.g. thickness-extension (TE) mode, become challenging at these frequencies, both due to dimensional consideration and possible interaction of different modes if the D/T-ratio is insufficiently large.

In the current work a free- and far-field three-transducer reciprocity calibration method has been modified to allow for corrections accounting for laboratory instrumentation, as well as corrections for attenuation in air and diffraction. The derivation of the three-transducer method, as well as the corrections, are based on [12]. It is the objective to investigate if the corrections applied to the measurements seem reasonable. The reliability of the corrections are given through juxtaposing the corrected measurements with a corresponding simulation.

Two separation distances, d, have been investigated in the current work, 0.40 m and 0.77 m. The latter for direct comparison with [12], and the former investigating the effects of moving the transmitter and receiver closer together.

In addition, due to the piezoelectric discs operating with the electrodes exposed there is a leakage of electromagnetic radiation (EMR) from the transmitter which is picked up by the receiver. The receivers sensitivity to this leakage is frequency dependent and increases with shorter spacing between the transmitter and receiver. The receivers sensitivity to this leakage could also in part be due to about 0.20 m of unshielded cable connecting the piezoelectric discs to the coaxial cable. An

investigation of the effects the EMR has on the SNR is undertaken, yielding two different SNR analyses obtained for two separation distances and two generator voltages. The results from the SNR analysis are used to highlight the frequency range where calibration can be expected to be performed with a SNR > 40 dB.

II. Theory

II.A. System model

A theoretical model, denoted system model, is introduced to describe the measurement system at hand. The system model is divided into several modules, represented by blocks. This division of the system model simplifies the theoretical description of the measurement system at hand.

In Fig. 1 the transmitting disc (left) and receiving disc (right) are shown in a coordinate system. The front face of the transmitting disc lies in the xy-plane at $z = 0$, centred at the z-axis. Similarly, the front face of the receiving disc lies in the xy-plane at $z = d$, centred at the z-axis. Both discs have radius a. The acoustic axis runs along the z-axis and d is the separation distance between the front faces of the transmitting and the receiving discs.

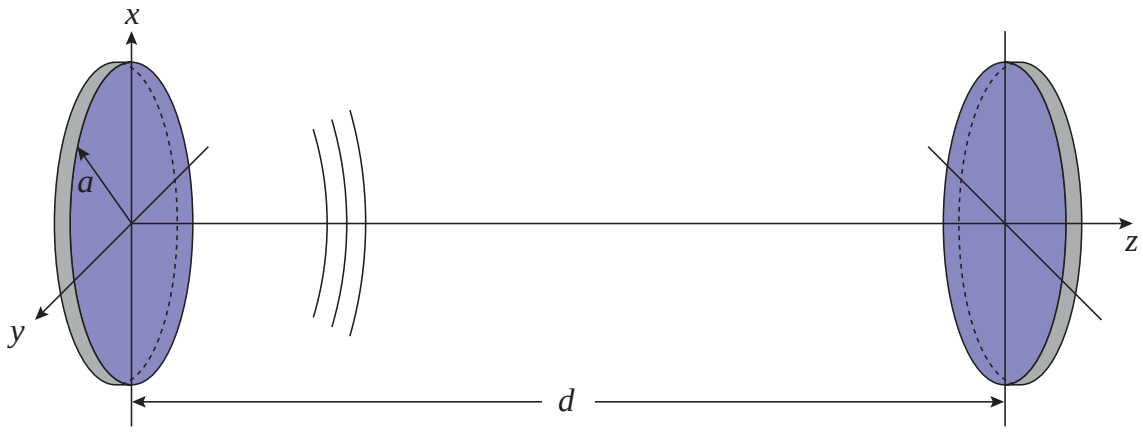

Figur 1: Schematics of coordinate system with transmitting disc (left) and receiving disc (right).

In Fig. 2 the block diagram of the system model is given. An explanation of the quantities involved are given below, and an explanation of the equipment represented by the individual blocks is given in Sec. III.A. All quantities in Fig. 2 are given as the Fourier transform of the time-domain equivalents, cf. Sec. III.B. Throughout, linear theory is used and the harmonic time dependency $e^{i\omega t}$ is assumed and suppressed, where $\omega = 2\pi f$, and f is the frequency. f is also suppressed from the quantities given in Fig. 2, e.g. $V_n = V_n(f)$, where n is any integer between 0 and 6.

V_0 is the voltage delivered to cable 1 from the function generator. V_{0m} is the recorded voltage from the function generator through cable 2. V_1 is the drive voltage over the terminals of the transmitting disc. u_2 is the particle displacement at the center of the face of the transmitting disc. $p_3 = p_3(d_0)$ is the on-axis free- and far-field sound pressure at a reference distance $d_0 = 1$ m. If d_0 is not in the far-field of the transmitting disc, the sound pressure is extrapolated back to the reference distance, d_0, from a pressure measured in the far-field [20]. $p_4 = p_4(d)$ is the on-axis free-field sound pressure at a separation distance d between the transmitting and receiving disc.

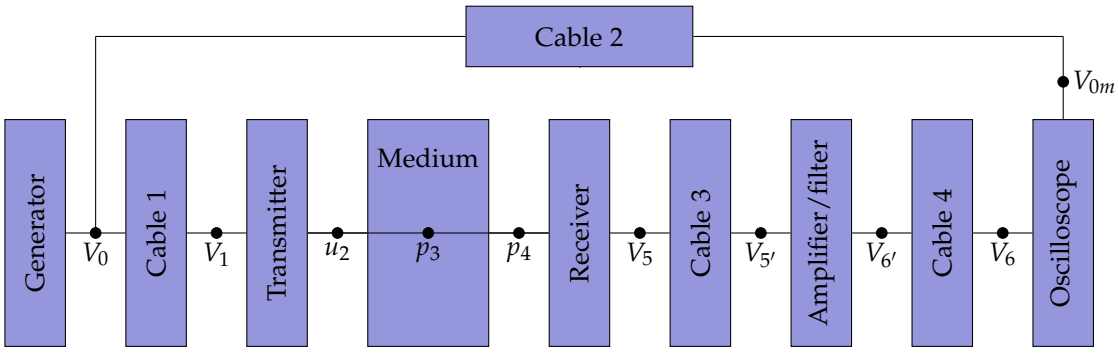

Figur 2: Functional block diagram of system model given in the frequency domain, i.e. all quantities are complex.

V_5 is the voltage delivered from the receiving disc to cable 3. V_5' is the input voltage across the terminals of the amplifier. V_6' is the voltage delivered to cable 4 by the amplifier. V_6 is the recorded voltage given the path just described.

In addition, V_{5open}, the open-circuit output voltage at the terminals of the receiving disc, $V_{6'open}$; the open-circuit output voltage at the terminals of the measurement amplifier; and, V_{gen}, the peak open-circuit generator voltage, corresponding to the peak electromotive force, are used.

II.B. Derivation of the free-field spherical three-transducer reciprocity method

The derivation follows the approach in [12], though with some minor changes in the notation; the derivation is repeated in the current work for completeness.

The conventional three-transducer reciprocity method [7] is modified to account for the transmitting voltage response [21], [12] rather than the transmitting current response.

In the derivation, it is assumed 1) that the receiving transducer is in the far-field of the transmitting transducer, 2) that free-field conditions exist at the location of the receivers front face 3) that the open-circuit voltage is recorded, 4) that the medium is without losses and 5) that at least one of the transducers involved are reciprocal, i.e. one transducer needs to be both linear and reversible.

In Fig. 3 the schematics of the modified three-transducer calibration method is given. T_1, T_2 and T_3 refers to the three transducers used, where T_1 is the transmitting transducer, T_2 is the transducer, or microphone, under investigation, and T_3 is the reciprocal transducer, used as both receiver and transmitter. The superscripts (1), (2) and (3) refer to measurements 1, 2 and 3, respectively. d_1, d_2 and d_3 are the separation distances between the transmitting transducers and the receiving transducers front faces, for the respective measurements.

The complex transmitting voltage response relates the on-axis, free- and far-field pressure at a reference distance $d_0 = 1$ m, to the voltage over the transducers electrical terminals [22]

$$S_V \equiv \frac{p_3}{V_1} = |S_V| e^{i\phi_{S_V}} \tag{1}$$

where $|S_V|$ is the magnitude and ϕ_{S_V} is the phase of the transmitting voltage response.

If the sound pressure is obtained at a distance, d, different than the reference distance, d_0, the

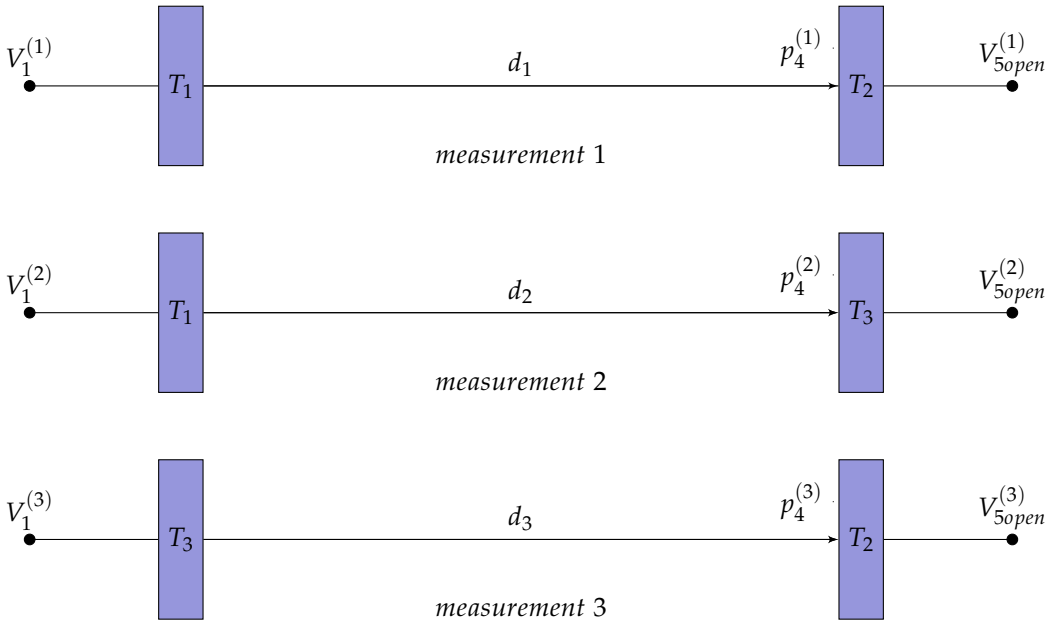

Figur 3: Schematics of the modified three-transducer calibration method.

corresponding sound pressure at 1 m is obtained by extrapolation

$$p_3 = p_4 \frac{d}{d_0} e^{ik(d-d_0)} \tag{2}$$

where $k = \omega/c$ is the wave number and c is the sound velocity of the medium at a frequency, f. Substituting p_3 in Eq. 1, yields

$$S_V = \frac{p_4}{V_1} \frac{d}{d_0} e^{ik(d-d_0)} \tag{3}$$

The complex receiving voltage sensitivity is the quotient of the output open-circuit voltage at the terminals of the receiving transducer to the on-axis free- and far-field sound pressure, given as [8]

$$M_V \equiv \frac{V_{5open}}{p_4} = |M_V| e^{i\phi_{M_V}} \tag{4}$$

where $|M_V|$ is the magnitude and ϕ_{M_V} is the phase of the receiving voltage sensitivity.

The complex spherical reciprocity parameter is the quotient of the receiving voltage sensitivity to the transmitting current sensitivity [23]

$$J \equiv \frac{M_V}{S_I} = \frac{M_V}{S_V Z} = \frac{2d_0}{i\rho f} e^{ikd_0} \tag{5}$$

where S_I is the transmitting current response, Z is the input electrical impedance of the transmitting transducer and ρ is the density of the medium.

The complex voltage to voltage transfer functions is defined as

$$H_{15open}^{VV\ (i)} \equiv \frac{V_{5open}^{(i)}}{V_1^{(i)}} \tag{6}$$

where $i = 1$, 2 and 3 refers to measurement 1 through 3, respectively.

From the above definitions the receiving voltage sensitivity of the transducer under investigation can be found as [12]

$$M_V^{T_2} = \left[J^{(3)} Z^{T_3} \frac{H_{15open}^{VV\ (1)} H_{15open}^{VV\ (3)}}{H_{15open}^{VV\ (2)}} \frac{d_1}{d_0} \frac{d_3}{d_2} e^{ik(d_1+d_3-d_0-d_2)} \right]^{\frac{1}{2}} \tag{7}$$

where $J^{(3)}$ is the spherical reciprocity parameter for measurement 3, and Z^{T_3} is the complex input electrical impedance of the reciprocal transducer, T_3.

II.C. Corrections

When performing measurements, the ideal conditions assumed in Sec. II.B are not generally fulfilled. Therefore, corrections have to be made on the recorded voltages to account for lack of ideal measuring conditions. Corrections are performed for 1) attenuation in air, 2) diffraction due to near-field effects, and 3) laboratory instrumentation, i.e. coaxial cables, signal amplifier and filter, termination of signal in oscilloscope and electrical impedance of the piezoelectric discs.

Correction 1) and 2) are theoretical corrections, while 3) is a mixture of theoretical corrections and corrections based on measurements. The corrections under 3) consist of voltage to voltage transfer functions relating the output voltage of a given block to the input voltage of the same block, cf. Fig. 2. Several blocks can be combined. The cables connecting the laboratory instruments are modelled as ideal transmission lines. For a supplementary discussion on the corrections, cf. [24], and [12], [13]

Measurement on the input impedance of a 2.97 m long coaxial cable connected to the input terminals of the B&K measurement amplifier has shown fair agreement with a simulation of the same combination. Though, some deviations were noticed, this did not transfer noticeably to the resulting quantity, M_V. All corrections for cables are in the current work obtained theoretically.

In [25] the absorption in air is given as

$$p_t = p_i e^{-0.1151 \cdot \alpha_{dB/m} \cdot z} \tag{8}$$

where p_i is an initial lossless sound pressure and p_t is the corrected sound pressure accounting for attenuation in air, $\alpha_{dB/m}$ is the absorption coefficient given in decibels per meter and z is the distance the sound wave propagates in air. Rewriting Eq. 8, yields the correction factor for attenuation in air [12]

$$C_\alpha \equiv \frac{p_i}{p_t} = e^{0.1151 \cdot \alpha_{dB/m} \cdot z} \tag{9}$$

The correction term for diffraction, C_{dif}, is based on Khimunin's diffraction correction [26] for a uniformly vibrating piston source mounted in a rigid baffle of infinite extent. This is considered as a simplification with regard to the piezoelectric discs used in the current work. The measured pressure is extrapolated out to a far-field axial distance, $z_{ff} = 1000$ m, before the corresponding on-axis far-field pressure is spherically extrapolated back to the measurement distance, d.

The correction term for diffraction is given in [12] as

$$C_{dif} = \frac{d_{ff}}{d} \frac{H^{dif}(d_{ff}, f)}{H^{dif}(d, f)} \tag{10}$$

where H^{dif} is the Khimunin's diffraction correction, see [12] for complete derivation.

The complex voltage to voltage transfer function, obtained from measurements, with correction terms, is given as

$$H^{VV}_{15open} = \frac{V_6}{V_{0m}} \frac{1}{H^{VV}_{0m1} H^{VV}_{5open5'} H^{VV}_{5'6'open} H^{VV}_{6'open6}} C_\alpha C_{dif} \tag{11}$$

where $H^{VV}_{0m1} \equiv V_{0m}/V_1$ is the transfer function relating the measured voltage, V_{0m}, to the voltage across the terminals of the transmitting disc, V_1; $H^{VV}_{5open5'} \equiv V_{5'}/V_{5open}$ is the transfer function relating the input voltage across the terminals of the signal amplifier, $V_{5'}$, to the open-circuit output voltage across the terminals of the receiving disc, V_{5open}; $H^{VV}_{5'6'open} \equiv V_{5'}/V_{6'open}$ is the transfer function relating the open-circuit output voltage of the signal amplifier, $V_{6'open}$, to the input voltage across the terminals of the signal amplifier, $V_{5'}$; $H^{VV}_{6'open6} \equiv V_{6'open}/V_6$ is the transfer function relating the recorded voltage, V_6, to the open circuit output voltage of the signal amplifier, $V_{6'open}$.

The expression for H^{VV}_{15open} from Eq. 11 is substituted in Eq. 7.

III. Methods

III.A. Experimental set-up

The current experimental set-up is based on [27], [28], [12] and [13]. Except for some modification it is the same experimental set-up as was used in [12] and [13], i.e the coaxial cables connecting the disc to the signal generator and signal amplifier are exchanged from type RG58 to RG-178, and a new set of piezoelectric discs are used.

The transmitter and receiver are Pz27 [29] piezoelectric discs of approximately radius 10 mm and thickness 2 mm. The discs have conducting wires soldered onto both electrodes and the wires are attached with shrinking plastic to a thin metal rod of diameter 1 mm and length 0.2 m, cf. Fig. 4 (b).

In Fig. 4 (a) the discs are shown suspended coaxially in the measurement cage with $d = 0.77$ m. The measuring cage is surrounded by sheets of plastic preventing possibly airflow and ventilation currents from interfering with the measurements. On the right, two stages for linear translation in the x- and y-direction can be seen, and on the left a stage for rotation is shown. At the time of writing the translation in the z-direction is done manually.

When coaxially aligning the discs, the discs are first brought together with only a millimetre or two separating them. The discs are then aligned such that the front surfaces are parallel with each other and perpendicular to the z-axis. The discs are then moved apart to the measurement distance and a measurement on the separation distance, d, is made with a measuring tape. The final measurement position is obtained by employing the x- and y-axis stages to move either the transmitter or the receiver until the voltage reading on the oscilloscope is maximized.

An Agilent 33220A function generator is used to produce a sinusoidal tone burst. A burst time, b_t is defined as the time duration where $V_{gen} \neq 0$, i.e. the length of the burst given in seconds. Two burst times have been used, $b_t = 0.8$ ms and $b_t = 1.2$ ms, for the separation distances $d = 0.40$ m and $d = 0.77$ m, respectively. In addition, two peak open-circuit generator voltages $V_{gen} = 1$ V

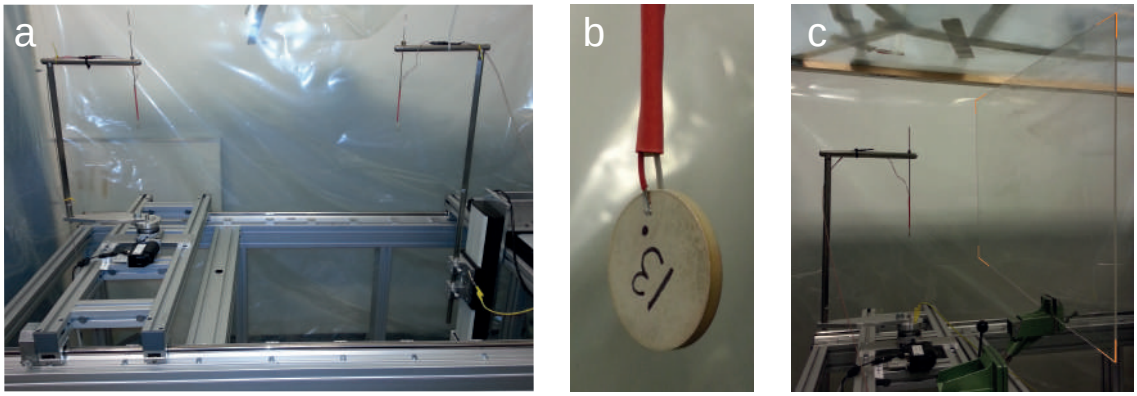

Figur 4: (a) Transmitting and receiving disc mounted in cage displaying how free-field conditions are approximately obtained. (b) Close up of Pz27 disc number 13 with polarization direction given as a black circle, cf. Fig. 1. (c) Acrylic plate mounted in front of the transmitter to block the acoustic energy from propagating.

and $V_{gen} = 10$ V have been investigated. A peak generator voltage of 10 V corresponds to 20 V peak-to-peak used in [12] and [13].

A Brüel and Kjær 2636 measurement amplifier, gain set to 60 dB, is used to amplify the received acoustical signal. The amplifier is connected to an external Krohn-Hite 3940A digital filter. The two signals, V_{0m}, and V_6, are recorded by a Tektronix DPO3012 digital oscilloscope. Temperature and humidity measurements are done with a Vaisala humidity and temperature transmitter, HMT313, for each frequency, and one or several manual readings of a barometer during measurements yields the atmospheric pressure. All connections between the laboratory equipment are done using coaxial cables and Matlab [30] is used to control the function generator and to read out the recorded voltages.

III.B. Signal processing

A fast Fourier transformation (FFT) [31] is utilized to obtain the peak-to-peak voltage of the transmitted and received bursts. From the recorded time-domain burst a shorter signal is obtained utilizing a rectangular window denoted FFT-window. The FFT-window is adjusted such that it will cut the signal in (or at the closest point to) zero for both the upper and lover frames, and it is applied towards the end of the transmitted and received bursts, where it is assumed that steady-state conditions are reached. The length of the FFT-window is determined from the number of sample points, N_{FFT}, approximately 20.000 and 30.000 samples given $b_t = 1.2$ ms and $b_t = 0.8$ ms, respectively; the total number of sample points in a recorded signal is 99.991. The windowed signal is zero-padded with an integer multiple of its own length, set to 10 times the windowed signal length. The transformation is given as

$$V_n(t) \overset{FFT}{\Leftrightarrow} V_{n_{ssp}}(f) \tag{12}$$

where $V_{n_{ssp}}(f)$ is the single-sided peak voltage spectrum obtained with Matlabs FFT-function and n is any integer between 0 and 6. From $V_{n_{ssp}}(f)$ the complex valued center frequency is read out for each burst and multiplied with 2·2 to obtain the complex peak-to-peak voltage, $V_n = V_n(f)$.

III.C. Finite element modelling

All finite element simulations are performed using FEMP 5.0, Finite Element Modelling of Ultrasonic Piezoelectric Transducers [32]. The simulation setup is defined in cylindrical coordinates and solved as a 2-dimensional, axisymmetric problem in the rz-plane, where $r = \sqrt{x^2 + y^2}$. The simulated piezoelectric disc is centred at the origin. All simulations are performed using infinite elements to represent the infinite fluid medium, where the infinite elements have been applied 30 mm radially from the origin in the rz-plane. 9 elements per shear wavelength, λ_s, have been used in the piezoelectric disc, while the medium, air, is simulated without losses using 9 elements per wavelength.

Since the material data obtained from Ferroperm comes with high uncertainty, an adjusted material data set have therefore been developed at UiB [17] and is used in the current work.

The derivation of the receiving voltage sensitivity obtained from a FE-based simulation model, is given in [24].

III.D. Noise analysis

Due to the discs operating with the electrodes exposed, it is observed that the piezoelectric discs are rather susceptible to electric energy, as well as acoustic. The observed electric energy is either 1) random fluctuations, or 2) coherent sinusoidal signals.

The random electric energy stems from electromagnetic fluctuations present in the laboratory, possibly due to computers and wireless communication as well as electric noise generated inside the laboratory equipment, e.g. thermal noise, shot noise and $1/f$ noise [33]. When recording the random electric energy, V_{gen} is set to zero. No coherent acoustic energy should therefore be present in the recording, though random acoustic energy might be present. Since no coherent signals are observed during the recording, this will be referred to as random noise.

The coherent sinusoidal signals stems from the transmitter which, when a sinusoidal voltage is superimposed across its terminals, sets up an electromagnetic field. This field is picked up by the receiver and will be referred to as EMR. This is an unwanted side effect of operating with discs rather than transducers, where an electromagnetic shield can be embedded in the design. It should be noted that no EMR is observed when recording with a Brüel and Kjær microphone system 4138-A-015.

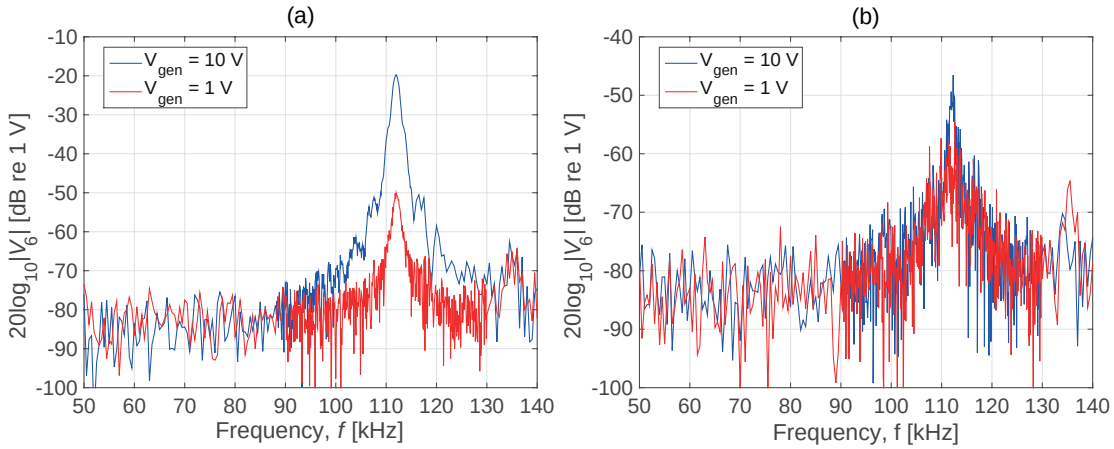

Figur 5: (a) Recorded coherent noise for $d = 0.40$ m and two generator voltages, V_{gen}, denoted in legend, (b) same as (a) but for $d = 0.77$ m.

To record the EMR an acrylic plate is mounted in front of the transmitter, cf. Fig. 4 (c). The recording of the EMR is then processed as in Sec. III.B, and in Fig 5 the results are given as a function of frequency for two separation distances and two voltages. Throughout the text, EMR recorded thus will be referred to as coherent noise. It should be noted that when recording the coherent noise, random noise is also present in the recording. Thus, in the absent of coherent noise e.g. for a large d or a low generator voltage, the recording of the coherent noise should converge to that of random noise.

In Fig. 5 (a) and (b) we see that from 50-90 kHz the voltage level for all curves flutters between -90 and -80 dB, corresponding to the voltage level of random noise. Exceeding 90 kHz, the coherent noise becomes significant when approaching 112 kHz, and increasingly so when the discs are positioned closer together. For $V_{gen} = 10$ V measured at d = 0.40 m, the voltage level at 112 kHz is about 1000 times larger than that of random noise, while the same comparison at $d = 0.77$ m yields a factor of about 32. Beyond 112 kHz, the voltage level reduces to that of random noise.

During some preliminary investigations on the possibility of using a Faraday cage to attenuate the electric noise, the coherent noise was successfully attenuated with a factor of about 2 without compromising the acoustical signal too much. More work will have to be done regarding this before any final conclusions might be reached.

It has been investigated if the peaks at 112 kHz might, in part or fully, be due to acoustic energy propagating through the acrylic plate. A simulation of an incident plane wave on an acrylic plate of thickness 4 mm yields a transmission coefficient at 112 kHz of about -120 dB. Thus it is assumed that all of the coherent noise stems from the EMR produced by the transmitter.

IV. Preliminary results

IV.A. Signal-to-noise ratio

In [7] it is stated that a SNR larger than 20 dB yields an error of about $\pm$ 1 dB in the calibrated quantity. This translates to about $\pm$ 10 percent error. In the context of calibration of measurement microphones, an error of about $\pm$ 10 percent is regarded as quite large, thus for the remainder of this work a criterion of SNR larger than 40 dB will be discussed. This corresponds to approximately $\pm$ 1 percent error. This does not guaranty that the final quantity, $M_V^{T_2}$, will be given with $\pm$ 1 percent error.

In Fig. 6 the SNR is plotted for two separation distances, d, and two generator voltages, V_{gen} for both coherent and random noise. Also, in the figures, are colour areas corresponding to the frequency range where the $\mathrm{SNR_r}$ for random noise (light blue area) and $\mathrm{SNR_c}$ for coherent noise (light red area) are greater then 40 dB. Due to the volatile behaviour of both $\mathrm{SNR_r}$ and $\mathrm{SNR_c}$, the exact frequency where the SNR is larger than 40 dB is difficult to pin down. These colour areas are inherited to, and used to analyse the results in, Fig. 7.

In Fig. 6 (a) a $\mathrm{SNR_r}$ larger than 40 dB is observed for a frequency range 65-120 kHz, yielding a frequency range of 55 kHz, peaking around 100 kHz with a peak level just below 80 dB. The $\mathrm{SNR_c}$ follows the same path as $\mathrm{SNR_r}$ from 50-90 kHz. From 90-112 kHz the $\mathrm{SNR_c}$ drops significantly compared to that of $\mathrm{SNR_r}$. Beyond 112 kHz the curves tend to converge, before at about 130 kHz they are overlapping. The frequency range where $\mathrm{SNR_c} > 40$ dB starts at 65 kHz ending at 105 kHz, yielding a frequency range of 40 kHz. The max deviation between the two curves, is observed at 112 kHz where $\mathrm{SNR_r}$ is 125 times larger than $\mathrm{SNR_c}$. 112 kHz corresponds to the frequency where the receiving disc is at its most sensitive.

In Fig. 6 (b) the same trend as in (a) is observed, though in (b) both frequency ranges are significantly more narrow. A $\mathrm{SNR_r}$ larger than 40 dB is observed for a frequency range 90-115 kHz

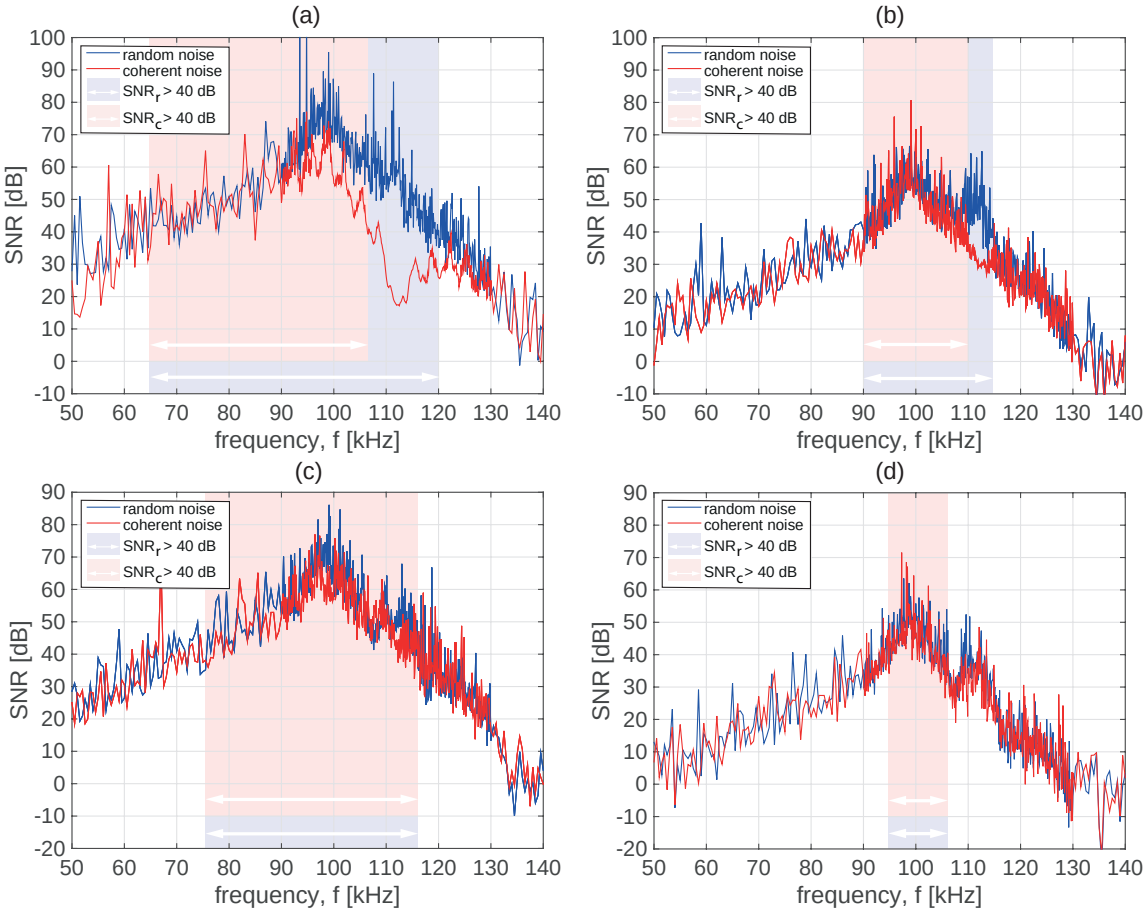

Figur 6: SNR for both random and coherent noise for two generator voltages voltages and two separation distances. (a) $V_{gen} = 10$ V, $d = 0.40$ m. (b) $V_{gen} = 1$ V, $d = 0.40$ m. (c) $V_{gen} = 10$ V, $d = 0.77$ m. (d) $V_{gen} = 1$ V, $d = 0.77$ m. The color areas denote the frequency range where the SNR given random noise, SNR_r, and SNR given coherent noise, SNR_c, are greater than 40 dB. The white arrows indicate the start and end of both frequency ranges.

while for SNR_c the frequency range is 90-100 kHz. Both curves are overlapping throughout the entire frequency range, except for 110-115 kHz. The peak SNR level, for both curves, is about 60 dB.

In (b) the upper limit of the $SNR_c > 40$ dB is located at 110 kHz, while in (a) the same upper limit is located at 105 kHz. Additional, the dip observed at 112 kHz in both (a) and (b) has a SNR_c level of 18 dB and 30 dB, respectively. Both indicatives that the effect of EMR relatively to the received acoustic energy, is less for 1 V than 10 V.

In Fig. 6 (c) a SNR larger than 40 dB is observed for a frequency range 75-115 kHz for both SNR_r and SNR_c Both curves are overlapping throughout the entire frequency range, with a slight deviation around 110-115 kHz. The peak SNR level, for both curves, is about 70 dB.

In Fig. 6 (d) a SNR larger than 40 dB is observed for a frequency range 95-105 kHz for both SNR_r and SNR_c In (d) Both curves are overlapping throughout the entire frequency range. The peak SNR level, for both curves, is around 50-55 dB.

Comparing the results from Fig. 6 (a) and (c), it is observed that the peak SNR_r level has

dropped from just below 80 dB to about 70 dB. This is in agreement with the received voltage level which increase with a factor of about 2, or 6 dB, when the discs are moved from $d = 0.77$ m to $d = 0.40$ m. Also, comparing the effects of coherent noise in Fig. 6 (a) with (c) it is observed the upper frequency with a $SNR_c > 40$ dB is shifted from 105 kHz to 115 kHz. The latter, indicating that the positive effect of an overall increased SNR is decreased due to the significant increase in EMR.

IV.B. Receiving voltage sensitivity, $M_V^{T_2}$

In Fig. 7 the measured receiving voltage sensitivity, $M_V^{T_2}$, for two separation distances, d, and two generator voltages, V_{gen}, are given as functions of frequency; the corresponding simulated receiving voltage sensitivity is given in red.

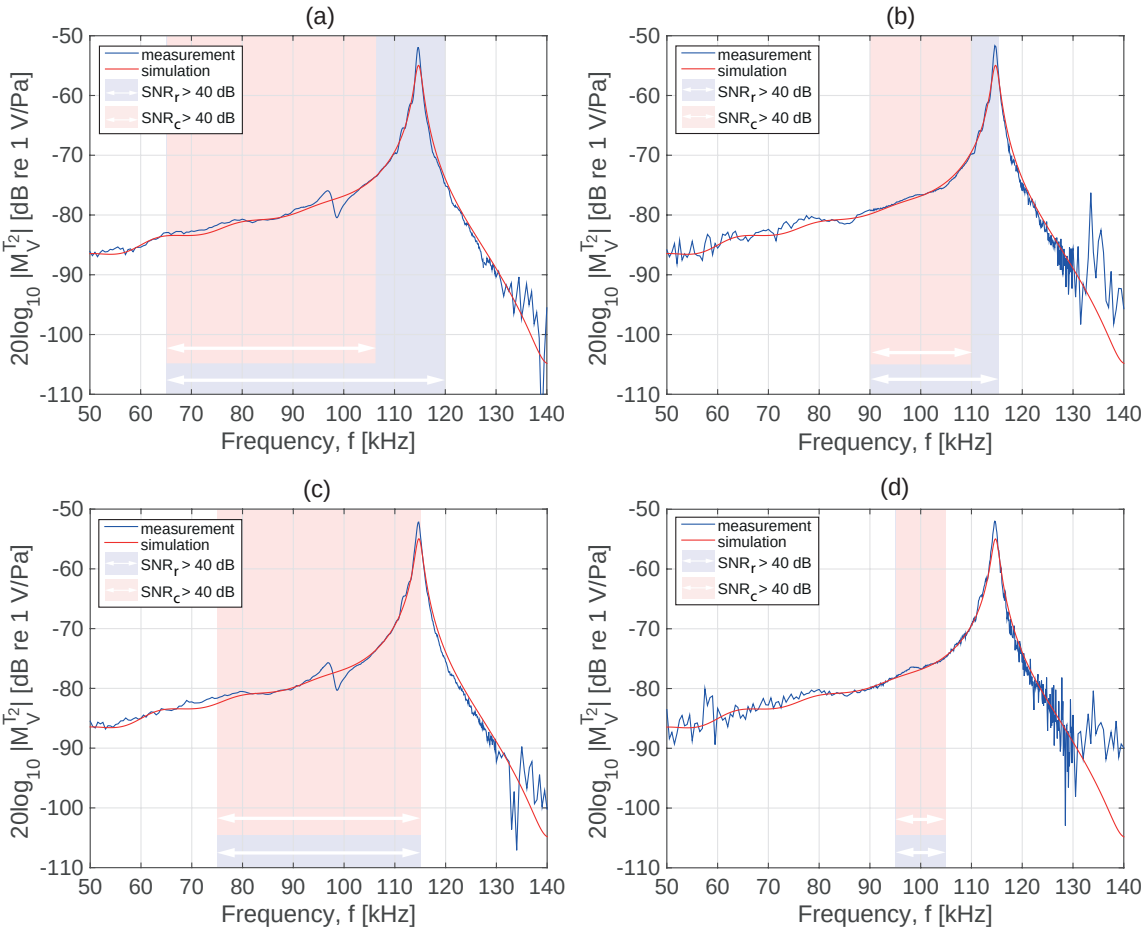

Figur 7: Receiving voltage sensitivity for two generator voltages and two separation distances. (a) $V_{gen} = 10$ V, $d = 0.40$ m. (b) $V_{gen} = 1$ V, $d = 0.40$ m. (c) $V_{gen} = 10$ V, $d = 0.77$ m. (d) $V_{gen} = 1$ V, $d = 0.77$ m. The colour areas are inherited from Fig. 6

In Fig. 7 (a) the measurement and the simulation show fair agreement throughout the frequency range except 1) at 112 kHz, where the measurement yield a value 3-4 dB higher than the simulation,

and 2) between 95-105 kHz where the non-linearity of the transmitting discs becomes evident [12], [13]. The first deviation is seen in all Figs. 7 (a) through (d). This deviation is thought to stem from the corrections for the receiving electronics. It is found that the correction for the receiving electronics depends largely on the electrical impedance of the receiving disc. It is not understood why the correction yields this deviation. The second deviation, due to the non-linearity of the transmitting disc, is seen only in Figs. 7 (a) and (c). The non-linearity of the piezoelectric disc becomes noticeable when approaching the series resonance frequency, approximately 100 kHz for $R1$, where the admittance of the disc increase.

The colour areas, inherited from Fig. 6, highlight the frequency ranges where we can expect to be able to perform calibration with a SNR > 40 dB. We clearly see how the coherent noise influence this frequency range, leaving the receiving voltage sensitivity peak of the $R1$ mode, at 112 kHz, out of range.

In Fig. 7 (b) the same agreement and deviation between the measurement and simulation, as in (a), can be observed. Though, at 95-105 kHz there is no visible deviation due to non-linearity. In the frequency range 50-90 kHz there is noticeably more noise present in the signal then in (a) and from 130 kHz to the end of the frequency range, it is seen that the signal is lost in the noise. When performing calibration, the blue area indicates that the peak at 112 kHz will partly be omitted considering random noise, and the red area indicates that same peak will mostly be excluded considering coherent noise.

In Fig. 7 (c) both deviations, as well as the same agreement between measurement and simulation, observed in a) can be seen. Both colour areas indicate that the peak at 112 kHz will partly be omitted when performing calibration.

In Fig. 7 (d) the same observations as was made for (b) can be made. Clearly, considering a SNR > 40 dB, the peak at 112 kHz will be omitted, leaving only the frequency range 95-105 kHz subject to calibration.

V. Discussion

The preliminary results on the receiving voltage sensitivity yields fair comparison with the finite-element based model [24], and with prior results obtained at UiB [12]. Though, some experimental challenges not experienced in [12] or [13] exist: 1) the random noise level is greater, observed especially when measuring with a generator voltage of 1 V, and 2) the deviation between the measured and simulated receiving voltage sensitivity at 112 kHz was not observed in [12] or [13].

The correction for attenuation in air, at 100 kHz, is 0.59 dB and 1.06 dB for separation distances 0.40 m and 0.77 m, respectively. The correction for diffraction effects, at 100 kHz, is 0.59 dB and 0.021 dB for separation distances 0.40 m and 0.77 m, respectively. The correction term for attenuation in air becomes more significant at larger separation distances and higher frequencies, while the the correction term for diffraction becomes more significant when the discs are moved closer together.

Choosing a measurement distance to be used during calibration is thus seen as a compromise between 1) a larger separation distance with less near-field effects followed by a reduction in the overall SNR level, and 2) a shorter separation distance which yields a greater overall SNR compromised by a severe increase in coherent noise and possibly also near-field effects.

Considering the current use of narrowband piezoelectric discs, the frequency range where we can expect to perform calibration with a SNR > 40 dB is regarded as fairly large. Although only piezoelectric discs have been investigated in the current work, at later stages it is the objective to apply the techniques considered here to in-house built transducers. It is also of interest to assess the reliability of the corrections described here through measurements with a pre-calibrated B&K

microphone system [12].

Furthermore, the preliminary results regarding SNR yields a substantial improvement from what was reported in [12] or [13]. The reason for the rather large deviation in the SNR analysis in this work compared to [12] or [13], stems from where the latter recorded the noise. In [12] or [13] the noise was recorded just before the acoustic burst arrived at the receiver, and no distinction was made between the coherent and random noise. Around 112 kHz the coherent noise present when the acoustic burst arrive might still be quite large.

VI. Preliminary conclusion

Except for the deviation between the measurement and simulation of M_V, observed at 112 kHz, all corrections performed seem reasonable and it appears justifiable to expand the three-transducer calibration method thus.

It may also be concluded that the effects of EMR need to be addressed when measuring with piezoelectric discs at shorter separation distances than 0.77 m.

VII. Acknowledgements

The present work is part of the first authors master thesis, due in Nov. 2015 [34]. The work is supported by The Michelsen Centre for Industrial Measurement Science and Technology. Furthermore, the authors thank the following persona for guidance and aid: Eivind Nag Mosland, Rune Hauge and Espen Storheim, Christian Michelsen Research, Bergen.

References

[1] P. Lunde, K.-E. Frøysa, R. A. Kippersund, and M. Vestrheim, "Transient diffraction effects in ultrasonic meters for volumetric, mass and energy flow measurement of natural gas," in *Proc. 21st International North sea flow Measurement Workshop*, Tønsberg, Norway, 28-31 October 2003.

[2] K.-E. Frøysa, P. Lunde, G. Lied, and A. Hallanger, "Natural gas quality measurements using ultrasonic flow meters. Development of a prototype Gas Analyzer with results from testing on North Sea gas field data," in *Proc. 30th Scandinavian Symp. on Physical Acoust.*, Geilo, Norway, 28-31 January 2007, Norwegian Physics Soc., http://www.norskfysikk.no.

[3] D. Reilly and G. Hayward, "Through air transmission for ultrasonic nondestructive testing," in *Proc. Ultrasonics Symposium, 1991.*, Dec 1991, pp. 763–766 vol.2.

[4] R. J. Bobber, *Underwater Electroacoustic Measurements*. Naval Research Laboratory Washington D.C., 1970.

[5] W. R. MacLean, "Absolute measurement of sound without a primary standard," *J. Acoust. Soc. Am.*, vol. 12, no. 1, pp. 140–146, 1940.

[6] R. K. Cook, "Absolute Pressure Calibrations of Microphones,"*J. Acoust. Soc. Am.*, vol. 12, pp. 415–420, 1941.

[7] *ANSI/ASA Procedures for Calibration of Underwater Electroacoustic Transducers*, ANSI/ASA Std. S1.20, 2012.

[8] *ANSI method for the calibration of microphones*, ANSI Std. S1.10, 1966 (R1976).

[9] *IEC Measurement microphones - Part 3: Primary method for free-field calibration of laboratory standard microphones by the reciprocity technique*, IEC Std. 61 094-3 ed1.0, 1995.

[10] M. J. Anderson, "Use of reciprocity to characterize ultrasonic transducers in air above 100 kHz," *J. Acoust. Soc. Am.*, vol. 103, no. August 1996, p. 446, 1998.

[11] ——, "Broadband electrostatic transducers: Modeling and experiments," *J. Acoust. Soc. Am.*, vol. 97, no. 1, p. 262, 1995.

[12] E. Mosland, "Reciprocity calibration method for ultrasonic piezoelectric transducers in air," Master's thesis, Department of Physics and Technology, University of Bergen, Norway, 2013.

[13] R. Hauge, "Finite element modeling of ultrasound measurement systems for gas. Comparison with experiments in air," Master's thesis, Department of Physics and Technology, University of Bergen, Norway, 2013.

[14] E. N. Mosland, R. Hauge, E. Storheim, P. Lunde, M. Vestrheim, and J. Kocbach, "Reciprocity calibration method for ultrasonic, piezoelectric transducers in air, including finite element simulations," in *Proc. 36th Scandinavian Symp. on Physical Acoust.*, Geilo, Norway, 3-6 February 2013, Norwegian Physics Soc., http://www.norskfysikk.no.

[15] E. N. Hauge, Rune and, E. Storheim, P. Lunde, M. Vestrheim, and J. Kocbach, "Finite element modeling of ultrasound measurement systems for gas. Comparison with experiments in air," in *Proc. 36th Scandinavian Symp. on Physical Acoust.*, Geilo, Norway, 3-6 February 2013, Norwegian Physics Soc., http://www.norskfysikk.no.

[16] R. Hauge, E. N. Mosland, E. Storheim, P. Lunde, M. Vestrheim, and J. Kocbach, "Updated results on finite element modeling of a transmit-receive ultrasound measurement system. Comparison with experiments in air," in *Proc. 37th Scandinavian Symp. on Physical Acoust.*, Geilo, Norway, 2-5 February 2014, Norwegian Physics Soc., http://www.norskfysikk.no.

[17] V. Knappskog, "Radiellmode svingninger i piezoelektriske ultralydstransdusere for luft. Målinger og endelig element analyse," Master's thesis, Department of Physics and Technology, University of Bergen, 2007, (in Norwegian).

[18] *Certificate of Calibration, No.: C1201771*, Brüel Kjær, 2012.

[19] M. Aanes, "Interaction of piezoelectric transducers excited ultrasound pulsed beams with a fluid-embedded viscoelastic plate," Ph.D. dissertation, Department of Physics, University of Bergen, Norway, 2014.

[20] L. E. Kinsler, A. R. Frey, A. B. Coppens, and J. V. Sanders, *Fundamentals of Acoustics*, 4th ed. John Wiley & Sons, New York, 2000.

[21] M. Vestrheim, "Phys272 - Akustiske transdusere," Lecture notes, Department of Physics and Technology, University of Bergen, Norway (in Norwegian), 2013.

[22] *ANSI Acoustical Terminology*, ANSI Std. S1.1, 1994.

[23] L. L. Foldy and H. Primakoff, "A General Theory of Passive Linear Electroacoustic Transducers and the Electroacoustic Reciprocity Theorem. I," *J. Acoust. Soc. Am.*, vol. 17, no. 2, pp. 109–120, 1945.

[24] A. A. Søvik, K. K. Andersen, P. Lunde, M. Vestrheim, and J. Kocbach, "Characterization of ultrasound transmit-receive measurement systems in air. Comparison of finite element modelling and experimental measurements," in *Proc. 38th Scandinavian Symp. on Physical Acoust.*, Geilo, Norway, 1-4 February 2015, Norwegian Physics Soc., http://www.norskfysikk.no.

[25] *ANSI Method for calculation of the absorption of sound by the atmosphere*, ANSI Std. S1.26, 1995.

[26] A. S. Khimunin, "Numerical Calculation of the Diffraction Corrections for the Precise Measurement of Ultrasound Absorption," *Acustica*, no. 27, pp. 173–181, 1972.

[27] Ø. S. Amundsen, "Material constants determination for piezoelectric disks, and influence on source sensitivity. Measurements and simulations," Master's thesis, University of Bergen, Department of Physics and Technology, Bergen, Norway, 2011.

[28] E. Storheim, "Diffraction effects in the ultrasonic sound field of transmitting and receiving circular piezoceramic disks in radial mode vibration. FE modeling and comparison with measurements in air," Ph.D. dissertation, University of Bergen, Department of Physics and Technology, Bergen, Norway, In preparation, 2015.

[29] *Meggit Ferroperm Piezoceramics*, Hejreskovvej 18 A, DK-3490 Kvistgård, Denmark, 2013.

[30] *The MathWorks, Inc.*, 3, Apple Hill Drive, Natick, Massachusetts 01760 USA.

[31] E. O. Brigham, *The Fast Fourier Transform and its application*, 1st ed. Prentice-Hall International Editions, 1988.

[32] J. Kocbach, "Finite Element Modeling of Ultrasonic Piezoelectric Transducers," Ph.D. dissertation, Department of Physics, University of Bergen, Norway, 2000.

[33] S. Kogan, *Electronic noise and fluctuations in solids*. Cambridge University Press, 1996.

[34] K. K. Andersen, "Working title: Reciprocity calibration method for ultrasonic piezoelectric transducers in air," Master's thesis, Department of Physics and Technology, University of Bergen, Norway, In preparation, 2015.